Journal of
Applied Crystallography

ISSN 0021-8898

Received 27 April 2011
Accepted 12 September 2011

Potential thermal expansion of calcitic and dolomitic marbles from Andalusia (Spain)

A. Luque,[a]* B. Leiss,[b] P. Álvarez-Lloret,[c] G. Cultrone,[a] S. Siegesmund,[b] E. Sebastian[a] and C. Cardell[a]

[a]Department of Mineralogy and Petrology, University of Granada, Faculty of Sciences, Granada 18071, Spain, [b]Geowissenschaftliches Zentrum der Universität Göttingen, Göttingen D-37077, Germany, and [c]Department of Geology, University of Oviedo, Oviedo 33005, Spain. Correspondence e-mail: analuque@ugr.es

Marble has historically been used as an ornamental stone because of its aesthetic appeal, ease of polishing and ex;cellent physical properties. One of the main factors affecting the durability of marbles is their thermal behaviour. Although marble is used extensively in Spain as a building and decorative material, little research has been done into its thermal behaviour. In this work, the textural and microstructural properties of seven calcitic and dolomitic marbles from Andalusia (southern Spain) were characterized to assess how these properties affect their thermal response. Rock fabric properties (grain morphology, boundaries and micro-crack populations) were studied by polarized microscopy and lattice preferred orientation using X-ray texture goniometry. Elastic properties were measured by ultrasound, thermal properties were determined by a six-rod dilatometer (thermal expansion) and the opening of micro-cracks was observed using environmental scanning electron microscopy. For each marble, thermal coefficients of calcite and dolomite crystals were calculated using thermo-X-ray diffraction, a novel application to characterize historic marbles. The results show that marble thermal expansion coefficients are related to preferred crystallographic orientation, which can help to identify the directions along which decay occurs. The results also show for the first time that the thermal expansion coefficient of the main components of marble, *i.e.* calcite and dolomite, is specific to each marble, and plays a key role in their different thermal behaviours. Thermal properties also depend on mineral composition, the existence of micro-cracks and hydric properties.

1. Introduction

Marbles are widely used as ornamental stone in modern buildings, historical monuments and statues. However, when exposed to the atmosphere, they sometimes undergo destructive and complex weathering phenomena, such as granular decohesion. Since Kessler (1919) found that repeated heating and cooling cycles caused the irreversible expansion of marbles, many other researchers have also focused on this aspect of decay (*e.g.* Rosenholtz & Smith, 1949; Zezza *et al.*, 1985; Royer Carfagni, 1999; Siegesmund *et al.*, 1999; Siegesmund, Weiss & Schegg, 2000). Logan *et al.* (1993) found that this phenomenon was a consequence of the anisotropic behaviour of calcite when heated, while Thomasen & Ewart (1984) and Bortz *et al.* (1988) studied the role of moisture in the mechanical deterioration of marbles. These last authors observed that some type of rocks used as cladding in building facades show hysteresis or a permanent deformation when they are exposed to several thermal cycles in the presence of moisture.

Monk (1985), in particular, considered that the water permeability of marble panels was crucial to their lack of durability, and Winkler (1996) explained that, in the presence of moisture, water molecules could enhance stone dilatation, causing cracks and flakes to develop, which leads to granular disintegration. This author also described how thermo-hydric fluctuations initiated the activity of other decay agents (*e.g.* salt solution, freezing water *etc.*), which can affect the internal structures of marble.

The mechanical behaviour of marble when exposed to changes in temperature depends on the anisotropic thermal expansion of calcite and dolomite crystals, the main mineral phases of this rock type. It is well known that an increase in temperature leads to a dilatation along the crystallographic *c*-axis direction of calcite and dolomite single crystals, a contraction along the *a*-axis direction of calcite crystals and an expansion along the *a* axis of dolomite crystals (Kleber, 1959; Reeder & Markgraf, 1986).

However, it has also been observed that some marbles behave differently when subjected to changes in temperature as a result of their different petrophysical properties (Rayleigh, 1934; Widhalm *et al.*, 1996; Leiss & Weiss, 2000;

Koch & Siegesmund, 2004). Siegesmund *et al.* (1999) proposed that the lattice preferred orientations (textures) of crystals and grain microstructure (morphology and geometry of the grain boundary) play a basic role in the thermal behaviour of marble. They also concluded that the early stage of marble decay is due to thermal weathering, which causes progressive granular decohesion. This process begins with the development of micro-cracks along fabric discontinuities, such as grain boundaries, cleavage planes and pre-existing cracks. This leads to an increase in porosity and a general loss of cohesion in the marble.

Zeisig *et al.* (2002) distinguished the following three types of thermal behaviour in different marbles when subjected to thermal tests: (i) isotropic thermal expansion coefficient and large residual strain; (ii) anisotropic thermal expansion coefficient and little or no isotropic residual strain; and (iii) anisotropic thermal expansion coefficient and anisotropic residual strain. These authors confirmed that marble thermal behaviour was partially controlled by the single-crystal properties (calcite and/or dolomite), and Siegesmund, Ullemeyer & Weiss (2000) stated that texture and other microstructural parameters determine the magnitude and directional dependence of the thermal expansion coefficient.

Microstructure-based finite element simulations were performed by Weiss *et al.* (2002, 2003) to determine the thermo-mechanical behaviour of calcitic and dolomitic marbles. They found that differences in marble textures (due to their composition) significantly affected the distribution of thermal stresses and suggested that texture was a key factor in determining marble durability. Marble is the only widespread rock type where the direction of the thermal expansion coefficient and the residual strain is directly controlled by the preferred crystallographic orientation (Weiss *et al.*, 2004).

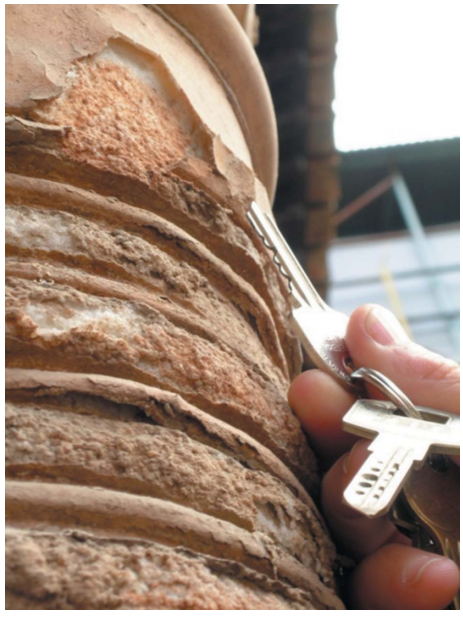

Figure 1
Detail of a marble column from the Courtyard of the Lions in the Alhambra (Granada, Spain), showing flakes and granular disintegration.

In recent decades Spain has been one of the world's main producers and exporters of marble. This material has been quarried since ancient times in different areas of Andalusia (Padilla, 1999), and archaeological research has uncovered numerous pieces made with marbles from Mijas (Malaga), Macael (Almeria), Aroche and Fuenteheridos (Huelva). In many cases, when these marbles are exposed to the environment for long periods, they can appear highly weathered (Bello *et al.*, 1992; Sáncho-Gómez, 2006; Álvarez de Buergo, 2008) (Fig. 1). Considerable research has been conducted into the physical properties of Andalusian marbles (Zezza & Sebastián-Pardo, 1992; Benavente *et al.*, 2007; Martínez-Martínez, 2008); nonetheless, thermal behaviour has not been considered a prominent factor in their decay.

However, because of thermal decay observed in some elements that compose the Lion Fountain (in the Alhambra of Granada), some specific research has been carried out recently to determine the thermal behaviour of white Macael marble when it is exposed to thermal changes (Sáez-Pérez & Rodriguez-Gordillo, 2009; Rodríguez-Gordillo & Sáez-Pérez, 2010; Luque *et al.*, 2010). Moreover, Luque *et al.* (2011) observed how three types of marble from Macael show different behaviour when they are submitted to thermal tests owing to the existence of differences in their mineralogical composition, fabric, grain size and shape, and the type of union among their crystals.

On the other hand, Benavente *et al.* (2008) noticed that the anisotropy of the linear expansion coefficient of the constituent minerals of ten types of porous stones and their relationship within the texture plays an important role in controlling the thermal expansion of stones. Also, Gómez-Heras *et al.* (2006) pointed out that thermal differences between minerals are significant since they magnify the effects that temperature gradients could produce on the mechanical breakdown of stones, especially in granites and other crystalline rocks.

Therefore, because of the importance of being able to predict the durability of marble when it undergoes thermal oscillations, this work tries to verify how this behaviour is directly conditioned by the mineralogy and physical properties of this type of monomineral rock.

The main objectives of this research are twofold: (i) to acquire a comprehensive knowledge of the fabric of the most common Andalusian marbles, and (ii) to understand how thermal oscillations may influence the decay of these marbles, especially when placed in buildings. Hence, the anisotropic thermal expansion, the rock fabric (grain size, grain boundary morphology, grain shape and micro-crack population) and the lattice preferred orientation (textures) of the different marbles were quantitatively analysed.

2. Materials

2.1. Marble types

Seven marbles from Andalusia were analysed: three from Sierra de los Filabres (Almeria) [white (WM), tranco (TM)

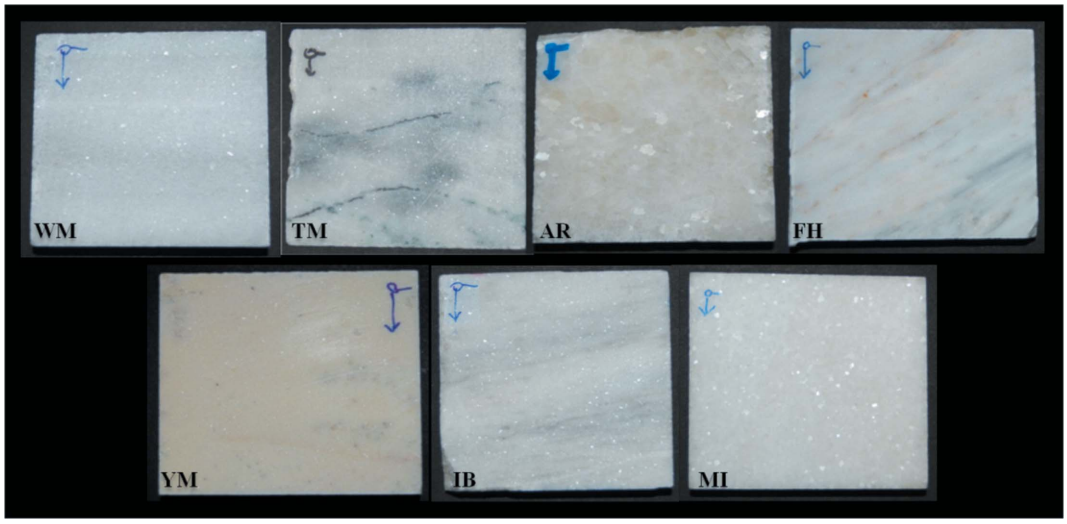

Figure 2
Photographs of polished specimens of the seven Andalusian marbles studied in this work (7 × 7 cm, *YZ* plane).

and yellow (YM) Macael]; two from Sierra de Aracena (Huelva) [Aroche (AR) and Fuenteheridos (FH)]; one from Sierra Tejeda (Granada) [white Iberico (IB)]; and one from Sierra Blanca (Malaga) [white Mijas (MI)] (Fig. 2).

Andalusian marbles can be grouped into three different geological districts (Luque *et al.*, 2010): the Nevado–Filabride complex (in which fall WM, TM and YM), the Alpujarride complex (IB and MI) and the Ossa Morena zone (AR and FH). Diverse metamorphic degrees have been identified in the above-mentioned marbles: low temperature and high pressure for WM, TM and YM; low temperature and medium-high pressure for IB; high temperature and high pressure for MI; high temperature and low pressure for AR; and medium-low temperature and low pressure for FH (Torres-Roldán, 1979; Díaz-Aspiroz *et al.*, 2004).

WM is a white calcitic marble with some parallel grey bands composed of opaque minerals (biotite, epidote, tremolite, zoisite and blue–green amphiboles). This marble also contains quartz, muscovite and albite (Sáez-Pérez, 2003). A visual inspection shows that the fabric is homogeneous and compact; the microstructure varies from granoblastic to xenoblastic with medium-sized grains (0.1–3 mm) and very few fissures.

TM is a calcitic marble with numerous parallel dark-grey bands composed of dolomite, pyrite, chalcopyrite, mica and apatite (Martínez-Martínez, 2008). Macroscale observation reveals a homogeneous fabric with compact homeoblastic microstructures composed of small to medium-sized grains (0.2–1.5 mm) and very few fissures.

YM is a yellow dolomitic marble with a heterogeneous fissured fabric and a homeoblastic texture. A few calcite crystals are present, mainly as a binder in the cracks. Some Fe and Mn oxides and hydroxides can also be found (Martínez-Martínez, 2008). The grain size (0.02–0.8 mm) is small compared to that of the other Macael marbles, and the only large grains (0.5–1 mm) are in the calcitic veins.

AR is an extremely heterogeneous calcitic marble characterized by a very coarse to medium-grained (0.4–4 mm) granoblastic microstructure. It is white with some green–grey veins. A compositional banding parallel to the foliation is defined by modal variations of diopside and phlogopite. Dolomite is irregularly distributed, and quartz and wollastonite appear as accessory mineral phases (Díaz-Aspiroz *et al.*, 2004).

FH is a white calcitic marble with small grain size (0.1–0.8 mm) and some marked heterogeneous green banding. This marble has a granoblastic microstructure and is characterized by the presence of quartz and dolomite as accessory or trace mineral phases (Espinosa *et al.*, 2002).

WI is a pure dolomitic white marble with numerous parallel dark-grey minerals bands (Sanz de Galdeano & López-

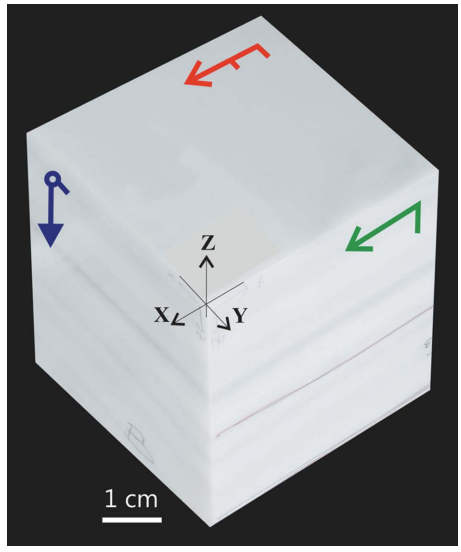

Figure 3
XYZ reference system of the samples oriented according to the macroscopic fabric elements, foliation and lineation. The red arrow follows the foliation plane and the direction of lineation; the blue arrow follows the direction of the *Z* axis (perpendicular to the foliation plane); the green arrow follows the direction of lineation (contained in the foliation plane).

Garrido, 2003). Macroscopically, the fabric is homogeneous, compact and granoblastic with small to medium grain sizes (0.2–1.5 mm). There are few fissures.

MI is a white dolomitic marble that occasionally shows blue or grey shades. Varying low amounts of plagioclase and organic matter can be found (Lapuente *et al.*, 2002). Macroscopically, the fabric is homogeneous with a compact heteroblastic microstructure and a bimodal grain size distribution (fine-grained and coarse-grained) (0.1–3.5 mm). There are few fissures.

The seven marbles can be divided into two main groups according to their mineralogical composition, namely calcitic (WM, TM, AR and FH) and dolomitic (YM, IB and MI) marbles.

3. Methodology

3.1. Petrographic characterization

In order to understand the spatial and geometric configuration of marble components in terms of fabric and microstructure, the method proposed by Passchier & Trouw (1996) was followed in this work. These authors used different terms (lineation and foliation, according to grain shape, grain size and grain boundary) to describe the geological history of rocks. The following parameters were considered: grain size distribution, grain aspect ratio, grain boundary geometry and lattice preferred orientation. The petrographic features of the marbles were observed by means of a polarized optical microscope (Olympus BX-60) coupled with a photomicrographic unit (Olympus DP10). This technique was used to identify the minerals and to characterize their microstructure (grain sizes and boundaries). Three thin sections normal to each other were prepared for each sample and analysed with parallel and crossed Nicols. A coordinate reference system (X, Y and Z axes) was applied in which the Z axis usually represents the normal of the foliation and the X axis, where possible, lies parallel to the lineation (Fig. 3).

3.2. Anisotropy of marbles

Because of their nondestructive nature, ultrasound velocity measurements are particularly useful for determining the physical properties of construction and ornamental materials. Measurements were performed with a Panametrics HV Pulser/Receiver 5058PR apparatus coupled with a Tektronix TDS 3012B oscilloscope. The ultrasound primary-wave (p-wave) velocity (Vp) was measured using the transmission method and nine measurements were made, three in each spatial direction (X, Y and Z).

The propagation velocity of compressional pulses was measured according to the ASTM (2005) D2845-05 standard test on dry (for 48 h at 298 K) and wet saturated (under high vacuum pressures) samples (three drilled cores of 15 mm diameter $\times$ 50 mm length in each marble spatial direction) using polarized Panametric transducers of 1 GHz. These data were used to infer information on the degree of compactness of the marbles as well as on the fabric anisotropy of the marbles (ΔM, in %), the value of which can be calculated as follows:

$$\Delta M = \left(1 - \frac{2\mathrm{Vp}_{\min}}{\mathrm{Vp}_{\max} + \mathrm{Vp}_{\mathrm{mid}}}\right) 100. \quad (1)$$

Here $\mathrm{Vp}_{\max}$ is the maximum, $\mathrm{Vp}_{\min}$ is the minimum and $\mathrm{Vp}_{\mathrm{mid}}$ is the intermediate value among the mean ultrasound velocities (in m s^{-1}) measured along the X, Y and Z axes (Guyader & Denis, 1986).

Vp values can be used to determine the intrinsic and extrinsic properties of marbles and, as a result, the structural anisotropy of these crystalline rocks. They are also useful for detecting the presence of micro-cracks, which are revealed by the differences between the Vp values measured in dry (low pressure) and in saturated (high pressure) conditions (Weiss *et al.*, 2000; Strohmeyer & Siegesmund, 2002*a*,*b*).

3.3. Thermal expansion coefficient of marbles

The thermal expansion coefficients (α, in 10^{-6} K^{-1}) of the marbles were measured using a six-rod dilatometer (Strohmeyer, 2003). This coefficient represents the ratio between the change in length of the sample after cooling to room temperature and its original length; in this work the temperature oscillated in one cycle from 293 to 363 K before cooling again to 293 K. Three drilled cores orientated according to the previously established axes (X, Y and Z), were cut and analysed. Although 363 K is an unrealistic temperature when considering the overheating of building surfaces under the sun, we chose this temperature range to achieve a suitable degree of deterioration in a short time (one thermal cycle) and to allow comparison of our data with those reported by other researchers (Rosenholtz & Smith, 1949; Koch & Siegesmund, 2004; Siegesmund *et al.*, 2008; Luque *et al.*, 2010, 2011).

The thermal expansion coefficient (α) was calculated according to the following equation:

$$\alpha = 1/l/(\Delta l\, \Delta T), \quad (2)$$

where Δl (in mm) is the change in length of the sample, l (in mm) is the initial length of the sample and ΔT (in K) is the temperature interval.

The thermal expansion ($\varepsilon_{\mathrm{rs}}$, in mm m^{-1}) represents the difference between the length of the marble sample after cooling to room temperature and the original sample length. It is defined as

$$\varepsilon_{\mathrm{rs}} = \Delta l_{\mathrm{rt}}/l_{\mathrm{r}}, \quad (3)$$

where Δl_{rt} (in mm) is the change in length of the sample after cooling to room temperature and l_{r} (in m) is the original length of the sample for a given temperature range.

3.4. Crystallographic preferred orientations of the marbles

Texture measurements were carried out on an X-ray texture goniometer specially designed for rock texture analyses (PANalytical X'pert System X-ray diffractometer; see Leiss & Ullemeyer, 2006). These measurements were made to relate

geometrically the lattice preferred orientation of the samples to the experimentally determined tensors for the anisotropic physical properties (anisotropic thermal expansion and ultrasonic p-wave velocity). A large X-ray beam size of up to 7 mm in diameter, high X-ray intensities and parallel X-ray optics were achieved using a bundle of glass fibre capillaries at the primary beam side. This configuration and a programmed sample measuring system allowed us to measure relatively large sample volumes within a reasonable time (25 min per pole figure). On the basis of five experimental pole figures (006, 110, 104, 012, 113) for each sample, a quantitative texture analysis was performed by calculating the orientation distribution function (ODF) using the WIMV algorithm (Matthies & Vinel, 1982) and the iterative series-expansion method (Dahms & Bunge, 1989). The bulk rock anisotropy of the thermal expansion coefficient and the ultrasound wave velocity, represented in equal area projections, were calculated by applying the Voigt averaging method (Bunge, 1985). To increase the number of crystals (*i.e.* sample volume) measured, pole figures were measured at up to 13 different spots on each sample (measuring 70 × 70 × 10 mm) for all three sample directions *X*, *Y* and *Z*. For the pole figure measurements, a 5 × 5° (tilt/rotation angle) grid was applied.

3.5. Direct observation of micro-crack development with environmental scanning electron microscopy

To observe the formation of new cracks in the marbles and the widening or closure of pre-existing cracks during one thermal cycle (293 to 363 to 293 K), an environmental scanning electron microscope (ESEM) equipped with a heating stage was used. The images were obtained on an FEI QUANTA 400 ESEM, which operates at an accelerating voltage of 20 kV. During heating, the SE-BSE (secondary electron/backscattered electron) detector–sample distance was set to ∼12 mm and the ESEM chamber pressure was set at 267 Pa water vapour. This water vapour pressure is equivalent to that of environmental air at 293 K and 15% relative humidity. Each sample was heated at an average rate of 4 (1) K min^{-1}. The thermal behaviour of the seven marbles was studied on a thin slab (400 µm) from the *ZY* plane.

3.6. Thermal coefficient of calcite and dolomite crystals

Thermal expansion coefficients (α) of calcite and dolomite crystals were measured by thermo-X-ray diffraction (TXRD). *In situ* XRD data were acquired using a Philips PW1710/00 X-ray diffractometer with a PW1712 communication card *via* an RS232 serial port, full-duplex controlled by the *XPowder PLUS* software (Martín-Ramos, 2004). The heating device consists of a halogen lamp (Philips Capsule-line Pro 75 W, 12 V) that heats the XRD chamber up to 503 K, a Pt-1000 probe for temperature monitoring (0.5 K precision) and a software-controlled thermostat with digital temperature selection. A detailed description of the TXRD method is provided elsewhere (Cardell *et al.*, 2007). In particular, these authors analysed the dehydration processes of mirabilite and epsomite minerals under increasing temperatures, showing that TXRD is a powerful analytical tool to study *in situ* temperature-induced phase transitions and crystalline processes in many research fields. In our work, powder grain size samples (∼100 µm) were prepared and three thermal tests were performed on each marble. XRD patterns were scanned over a 2θ range from 20 to 60°, with 0.1° goniometric angle steps and 0.4 s integration time. A continuous scan mode was applied by using Cu $K\alpha$ radiation. The voltage was 40 kV and the tube current 40 mA. The backgrounds of the diffraction patterns were subtracted. Diffraction patterns were collected and thermal expansion coefficients were calculated by measuring the change in length in the direction of each crystallographic parameter of the unit cell (*a*, *b* and *c*) with increasing temperature. Problems with the cooling system used to stabilize the water temperature at 298 K forced us to perform the test in a temperature range of 303–363 K and with a 5 K min^{-1} heating rate.

Table 1
Main microstructural parameters for the seven Andalusian marbles.

		Fabric	Grain size (mm)	Grain shape	Grain boundaries	Twin types
Calcitic	WM	Grbl	0.1–3	Eq, Polyg	Straight	I–II
	TM	Hombl	0.2–1.5	Inq, Sub-ang	Embayed	II–III
	AR	Porfido-Grbl	0.4–4	Inq, Decus	Serrated	III–IV
	FH	Grbl	0.1–0.8	Eq, Round	Lobate	II
Dolomitic	YM	Hombl	0.02–1	Eq, Sub-round	Lobate	I
	IB	Grbl	0.2–1.5	Eq, Sub-ang	Embayed	II–III
	MI	Heterobl	0.1–3.5	Eq, Decus	Serrated	I–II

Fabric abbreviations: Grbl: granoblastic; Hombl: homeoblastic; Heterobl: heteroblastic. Grain shape abbreviations: Eq: equidimensional; Inq: inequidimensional; Polyg: polygonal; -ang: -angular; Decus: decussate; Round: rounded. Twin types according to Burkhard (1993).

4. Results and discussion

4.1. Petrographic characterization

Table 1 shows the microstructural properties of the Andalusian marbles studied. There are marked differences in terms of crystal shape and size, grain boundaries, and twinning, which indicate different metamorphic degrees, deformation processes and post-deformative recrystallization. According to Burkhard (1993), twins can be used to correlate the temperatures (*T*) at which deformation occurs during metamorphism processes. Thus four different types of twin can be distinguished: type I ($T < 473$ K), type II ($423 < T < 573$ K), type III ($T > 473$ K) and type IV ($T > 523$ K). According to this classification, our marbles fit their geological setting well (described above), with YM and FH having the lowest metamorphic degree and AR and MI the highest. Although all marbles are highly compact, visible fabric differences can be observed in marbles quarried from the same lithostratigraphic unit. This is due to differences in physical and mechanical properties as a consequence of local or regional variations in their tectonometamorphic history (Paterson & Weiss, 1961; Wenk *et al.*, 1973; Siegesmund *et al.*, 1999). The microstructural differences between the samples are shown in Fig. 4. Samples WM and MI show the largest crystal sizes, while

samples AR, TM and IB have medium crystal sizes, and samples FH and YM have the smallest sizes. Differences in grain boundary geometries of all marbles can also be observed (*e.g.* WM shows straight grain boundaries, TM and IB are embayed, AR and MI are serrated, and FH and YM are lobate).

4.2. Anisotropy of the compressional ultrasound wave velocities of marbles

Table 2 summarizes the ultrasound p-wave velocity for dry and water-saturated samples and the anisotropy values of the seven marbles. Considering the Vp values measured by Dandekar (1968) in single calcite (Vp_{max} = 7730 m s^{-1} and Vp_{min} = 5710 m s^{-1}) and dolomite crystals (Vp_{max} = 8450 m s^{-1} and Vp_{min} = 6280 m s^{-1}), the values obtained in this work for dry samples are generally lower, while the values obtained for the saturated samples are always closer to the single-crystal values (Table 2). The highest velocities were for the dolomitic marbles (YM, IB and MI).

Vp values measured in dry samples showed a higher degree of anisotropy than the saturated samples. The dry sample with the highest anisotropy was FH (27%), followed by YM (22%), while the least anisotropic sample was AR (6%). The saturated samples did not always show the same tendency. According to Strohmeyer & Siegesmund (2002*a*,*b*), the difference ΔVp ($Vp_{saturated}$ − Vp_{dry}) can provide an insight into crack-induced anisotropy. This is because the open-crack effect is reduced though not completely eradicated in saturated samples, since the compressibility of air (which governs Vp_{dry}) is higher than that of water ($Vp_{saturated}$). When Vp is measured in marble in dry conditions (low pressures), the micro-cracks and pore spaces are open. This means that the velocity anisotropy is a result of the oriented micro-cracks and the preferred orientations of anisotropic rock-forming minerals. The ΔVp values suggest that FH and YM marbles are more influenced by previously existing micro-cracks, whereas the values for IB and AR indicate that there were no pre-existing micro-cracks.

Table 2
Velocity of compressional pulses (Vp in m s^{-1}) in dry and saturated samples in the three (*X*, *Y* and *Z*) perpendicular directions.

Δ*M* (%) indicates the anisotropy of each marble.

Calcitic		Vp (m s^{-1})		Dolomitic		Vp (m s^{-1})	
		Dry	Saturated			Dry	Saturated
WM	*X*	5885	6405	YM	*X*	6597	7452
	Y	5756	6386		*Y*	6573	7304
	Z	5058	6246		*Z*	5165	6816
	Δ*M* (%)	13.10	2.34		Δ*M* (%)	21.56	7.62
TM	*X*	6210	6589	IB	*X*	5146	7044
	Y	5678	6253		*Y*	4348	6772
	Z	5387	6073		*Z*	4298	6766
	Δ*M* (%)	9.37	5.42		Δ*M* (%)	9.46	2.06
AR	*X*	5061	6185	MI	*X*	5299	7436
	Y	4705	5952		*Y*	4841	7325
	Z	4971	6024		*Z*	5966	7514
	Δ*M* (%)	6.20	2.50		Δ*M* (%)	14.05	2.01
FH	*X*	4055	6588				
	Y	4513	6640				
	Z	3129	6456				
	Δ*M* (%)	26.96	3.12				

4.3. Anisotropy of the thermal expansion coefficient of marbles

Table 3 shows the thermal expansion coefficients (α) and residual strain (*r*) measured along the *X*, *Y* and *Z* orthogonal directions of the seven marbles during one thermal cycle (293–

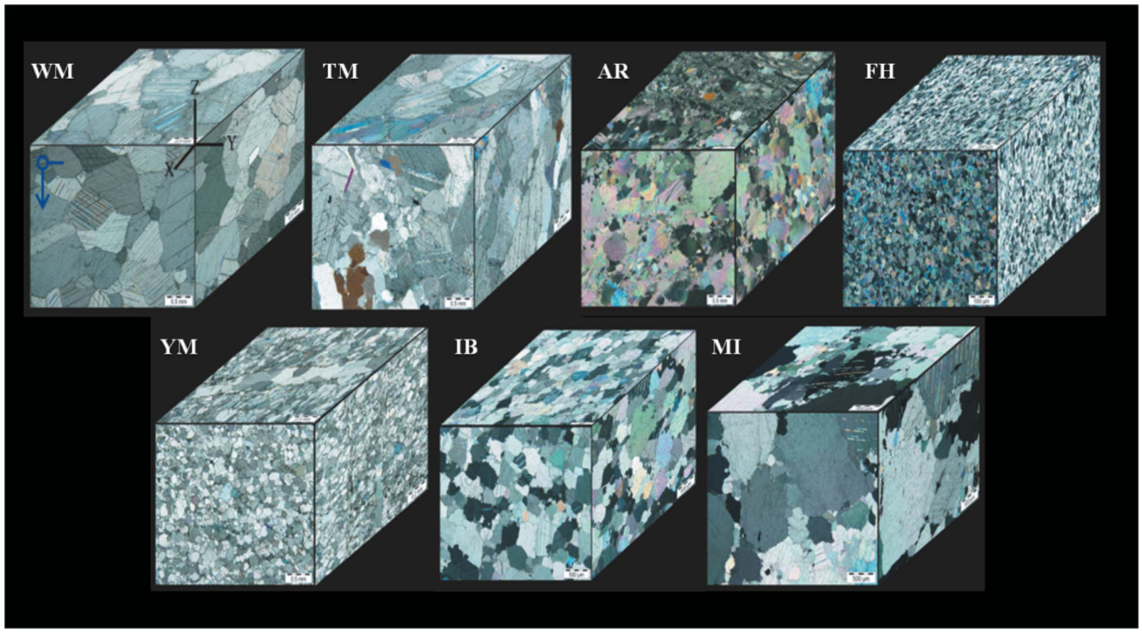

Figure 4
Microstructure of the marbles represented by thin sections of the *XY*, *XZ* and *YZ* planes.

Table 3
Thermal expansion coefficient (α) and residual strain (r) of the seven Andalusian marbles.

Calcitic		α (10^{-6} K^{-1})	r (mm m^{-1})	Dolomitic		α (10^{-6} K^{-1})	r (mm m^{-1})
WM	*X*	16.67	0.31	YM	*X*	12.91	0.01
	Y	9.52	0.09		*Y*	13.34	0.01
	Z	23.97	0.29		*Z*	16.57	0.07
TM	*X*	4.66	0.08	IB	*X*	5.65	0.01
	Y	10.69	0.06		*Y*	8.01	−0.02
	Z	13.92	0.13		*Z*	11.60	−0.02
AR	*X*	4.22	0.03	MI	*X*	13.36	−0.02
	Y	6.72	0.05		*Y*	10.46	0.01
	Z	16.42	0.01		*Z*	8.80	−0.01
FH	*X*	7.45	0.05				
	Y	8.00	0.03				
	Z	12.26	0.06				

363–293 K) in dry conditions. The WM, YM and AR samples display the highest α values in the *Z* direction (α = 24, 17 and 16 × 10^{-6} K^{-1}, respectively), while the other marbles (TM, FH, IB and MI) show lower values, particularly MI (α = 8.8 × 10^{-6} K^{-1}). The results for residual strain reveal a different trend, however, with only the WM (0.29 mm m^{-1}) and the TM (0.13 mm m^{-1}) marbles showing high values. In the other marbles (AR, FH, YM, IB and MI) the residual strain is almost zero (below 0.07 mm m^{-1}).

It was also observed that the α_{max} values for the WM, TM, FH, YM and IB marbles run in the same direction as the Vp_{min} value measured in dry and saturated samples. This suggests that the preferred crystallographic orientation of the calcite or dolomite *c* axis could be parallel to the *Z*-axis direction of these marbles. Nevertheless, AR and MI marbles show different behaviour for Vp_{min} along their *Y*-axis directions with regard to their α_{max} values along the *Z*- and *X*-axis directions, respectively. On the other hand, it was found that thermal expansion coefficient values (α) obtained with the six-rod dilatometer in each marble sample were partially linked to the crystallographic preferred orientations of these marbles.

4.4. Crystallographic preferred orientations of marbles

Fig. 5 displays the results of the texture analyses by means of pole figures recalculated from an ODF. According to the classification proposed by Leiss & Ullemeyer (1999), the texture of the WM, AR, FH, YM and MI marbles can be defined as *c*-axis fibre type, since the *c*-axis maxima form single maxima, while the *a*-axis maxima are quite regularly distributed on a great circle. The *c*-axis maxima of these marbles are of moderate intensity and are sub-normally oriented with respect to the regional foliation. In contrast, TM and IB marbles can be defined as *a*-axis fibre types since one of the *a* axes forms the rotation axis for the great circle distribution of the *c* axis.

Thermal expansion coefficients (α) and ultrasonic wave velocities (Vp) were calculated from the ODF results and are represented in equal-area projections next to the pole figure plots for all samples (Fig. 5). Although α was calculated by the Voigt averaging method, it is quite low compared to the value

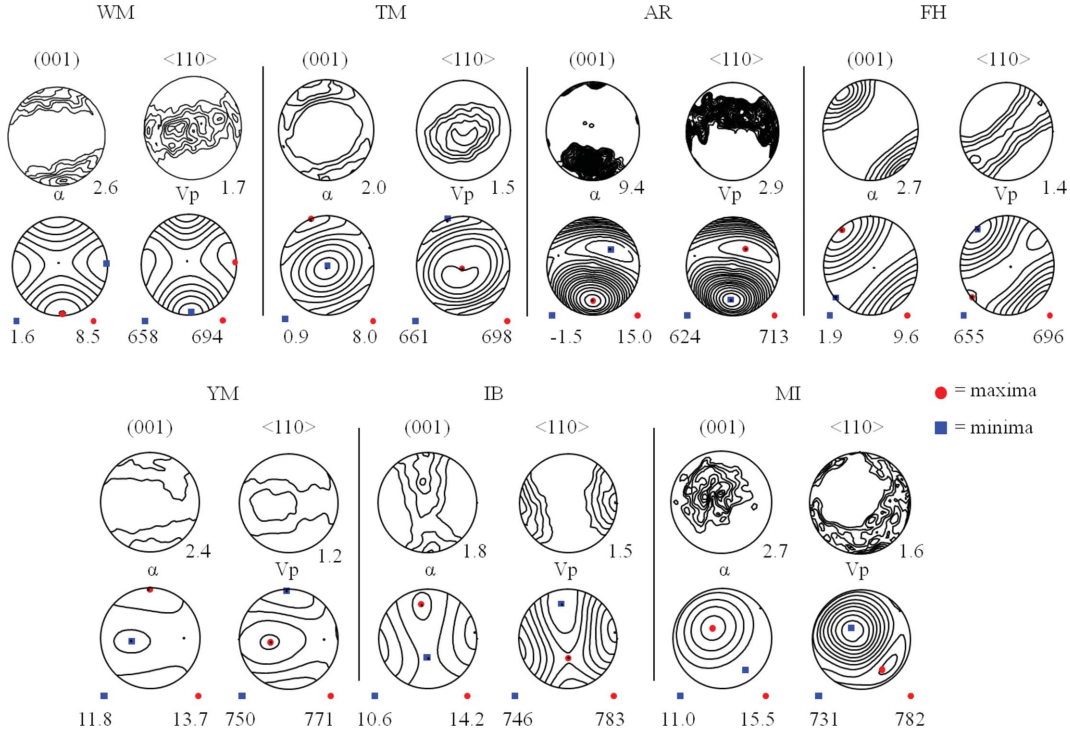

Figure 5
Upper row: Pole figures of the preferred orientations of the *c*(001) axes and *a*⟨110⟩ axes (*YZ* section as projection plane, equal-area projection, lower hemisphere, maxima are multiples of the random distribution = m.r.d.). Lower row: texture-based calculations of the thermal expansion coefficients (α) and velocities of compressional pulses (Vp).

Table 4
Thermal expansion coefficient (α) and velocities of compressional pulses (Vp) of the seven Andalusian marbles calculated using the Voigt averaging method.

Calcitic				Dolomitic			
		α (10^{-6} K^{-1})	Vp (m s^{-1})			α (10^{-6} K^{-1})	Vp (m s^{-1})
WM	*X*	3.5	6860	YM	*X*	12.0	7690
	Y	1.6	6950		*Y*	12.3	7650
	Z	8.5	6590		*Z*	13.7	7510
TM	*X*	0.9	6940	IB	*X*	13.5	7520
	Y	5.5	6760		*Y*	10.7	7820
	Z	7.5	6630		*Z*	13.9	7480
AR	*X*	3.1	6920	MI	*X*	14.8	7360
	Y	0.0	7070		*Y*	11.6	7720
	Z	11.0	6510		*Z*	11.6	7720
FH	*X*	2.9	6930				
	Y	5.1	6810				
	Z	6.3	6740				

obtained from direct measurement of marbles. By contrast, though the Vp values calculated from isolines show higher values, they fit better with the direct measurements of the saturated marbles (Table 4).

The texture-derived values for α and Vp show the same trend for all marbles. The highest α values are clearly correlated with the lowest Vp values and *vice versa*. It was also observed that, with the exception of AR and MI, the Vp_{min} calculated from isolines runs in the same direction as the Vp_{min} measured directly in WM, TM, FH, YM and IB. However, with the exception of sample WM, the *c*-axis maxima directions do not coincide with our coordinate directions *X*, *Y* and *Z*. This means that, with the exception of the WM sample, the calculated maximum and minimum α and Vp values cannot be directly compared with the experimental values that were determined parallel to our coordinate system.

4.5. Direct observation of micro-crack development with environmental scanning electron microscopy

By using hot-stage environmental scanning electron microscopy it was possible to directly observe the evolution of the micro-crack system in the marble during thermal cycles. ESEM images were obtained using the same temperature range used in the thermal expansion test (from 293 to 363 K and down again to 293 K). At 293 K no modifications were observed; however, when the temperature reached 363 K, grain boundaries opened within some marbles and intragranular micro-cracks developed. Nevertheless, in most marbles the micro-cracks closed again when the temperature diminished to 293 K.

As can be seen in Fig. 6, WM and FH marbles display the greatest opening of micro-cracks at 363 K (Figs. 6*a*.2 and 6*d*.2). These new micro-cracks are wider in the case of FH (~3 µm wide), although they were never more than 40 µm long. Nevertheless, when the sample returned to room temperature (293 K), the gap between crystals closed again (Fig. 6*d*.3). In WM, new micro-cracks of a few micrometres wide (~0.5 µm) opened. These cracks were over 75 µm long and remained open when the temperature returned to 293 K (Fig. 6*a*.3).

The other marbles, with the exception of IB, showed slight changes during the thermal cycle. When the temperature rose to 363 K some fractures (light tension lines) were detected, although at the end of the thermal cycle, when the temperature returned to 293 K, the cracks and fissures closed again (Fig. 6 series *b* and *c*, and Fig. 7 series *a* and *b*). Minimal changes were observed in the IB marble when the temperature reached 363 K, except for a smooth brightness along grain boundaries (Figs. 7*b*.1–7*b*.3). When the samples returned to their initial temperature, all lines and fissures disappeared. We suggest that, even in marbles with a strong anisotropy (*i.e.* large thermal expansion), crystal size and boundary configuration can influence the development of preferentially oriented micro-cracks and, as a consequence, their thermally induced decay (Zeisig *et al.*, 2002; Weiss *et al.*, 2002). The results revealed that micro-cracks opened only in WM and FH when the temperature reached 363 K; moreover, WM was the only marble where these cracks remained open at the end of the thermal test.

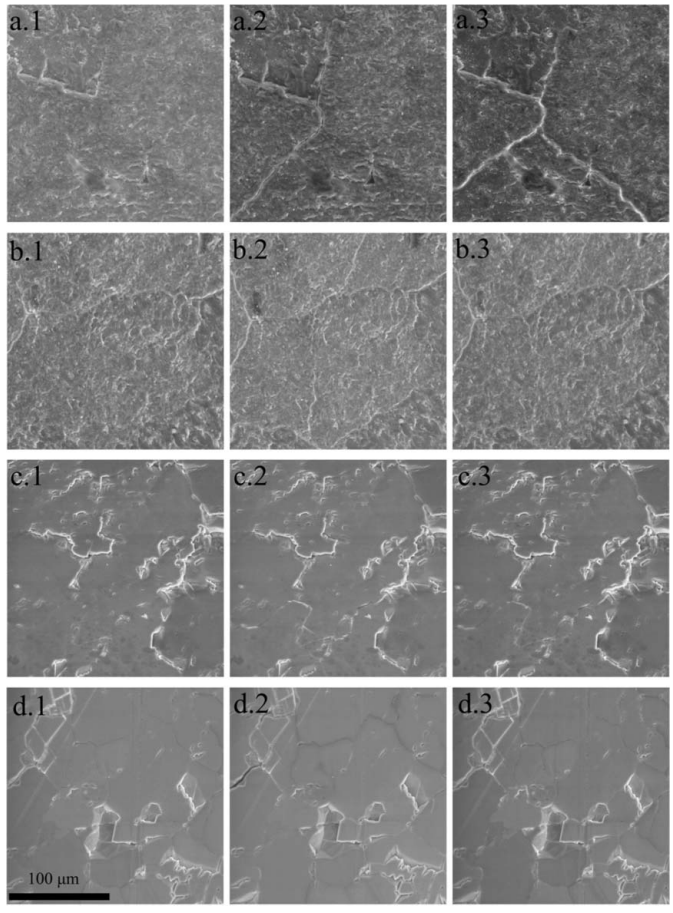

Figure 6
ESEM (with detector SE-BSE) images of calcitic marble surfaces during thermal cycles in the microscope chamber. Slight changes can be observed in the crack system during the increase in temperature (1: 293 K, 2: 363 K, 3: 293 K) in the four marbles. (*a*) WM, (*b*) TM, (*c*) AR (Aroche) and (*d*) FH (Fuenteheridos).

4.6. Thermal coefficient of calcite and dolomite crystals

An increase in temperature leads to the anisotropic thermal expansion of marble as a consequence of the anisotropic thermal expansion of calcite and dolomite single crystals (Kleber, 1959; Fredrich & Wong, 1986; Leiss & Weiss, 2000; Weiss *et al.*, 2004). Both single crystals (calcite and dolomite) show a positive dilatation along their crystallographic *c* axis ($\alpha = 26 \times 10^{-6}$ and $25.8 \times 10^{-6}\ K^{-1}$), whereas for the dilatation of the *a*-axis directions dolomite shows a weak expansion ($\alpha = 6.2 \times 10^{-6}\ K^{-1}$) and calcite shows a contraction ($\alpha = -6 \times 10^{-6}\ K^{-1}$) (Markgraf & Reeder, 1985; Reeder & Markgraf, 1986).

The thermal behaviour of a marble is closely related to the thermal behaviour of its single crystals, *i.e.* calcite and dolomite. However these crystals do not have the same crystal structural parameters (unit cell) as the corresponding pure single crystals ($a = 4.988$, $b = 4.988$ and $c = 17.061$ Å for calcite, and $a = 4.815$, $b = 4.815$ and $c = 16.119$ Å for dolomite) (Steinfink & Sans, 1959; Markgraf & Reeder, 1985). In fact, variable incorporation of Mg and/or Ca ions and other trace elements (Mn, Sr, Fe *etc.*), the existence of dislocations, and the metamorphic processes may affect the crystal lattice structure of the crystals (calcite and dolomite) that make up marbles (Althoff, 1977; Hartley & Mucci, 1996; Sternbeck, 1997; Wogelius *et al.*, 1997; Titiloye *et al.*, 1998) and consequently influence their anisotropic thermal properties. Therefore, to evaluate the crystallographic parameters of calcite and dolomite minerals and to determine how they vary with increased temperature, TXRD tests were performed.

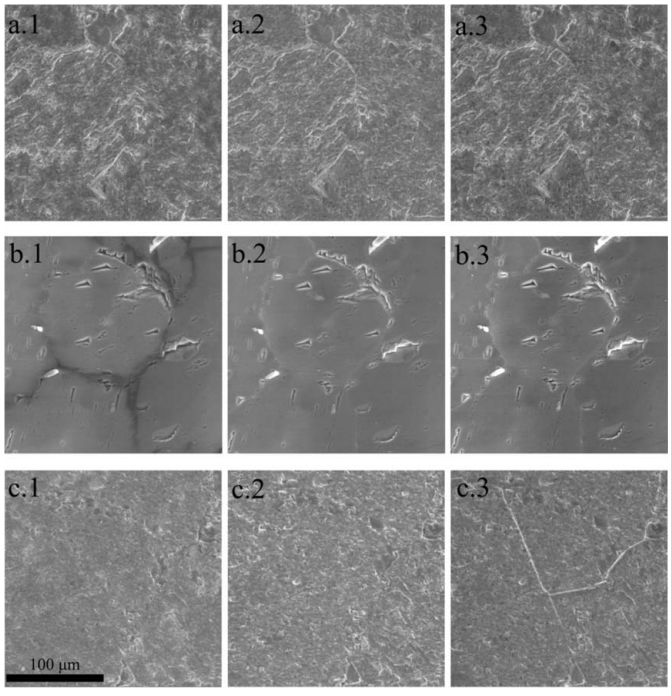

Figure 7
ESEM (mode SE-BSE) images of the dolomitic marbles surfaces during thermal cycles in the microscope chamber. Slight changes can be observed in the crack system during the increase in temperature (1: 293 K, 2: 363 K, 3: 293 K) in the three marbles. (*a*) YM, (*b*) IB and (*c*) MI.

Table 5
Lattice parameters of calcitic and dolomitic marbles at 303 and 363 K.

The thermal expansion coefficient α is also calculated for each parameter.

Calcitic		*a*/*b* (Å)	*c* (Å)	Dolomitic		*a*/*b* (Å)	*c* (Å)
WM	303 K	4.9826	16.9722	YM	303 K	4.8078	16.0427
	363 K	4.9841	16.9984		363 K	4.8104	16.0521
	α ($10^{-6}\ K^{-1}$)	5.02	25.70		α ($10^{-6}\ K^{-1}$)	9.01	9.77
TR	303 K	4.9700	16.9200	IB	303 K	4.7886	15.8854
	363 K	4.9160	16.9460		363 K	4.7930	15.9045
	α ($10^{-6}\ K^{-1}$)	5.37	25.60		α ($10^{-6}\ K^{-1}$)	15.30	20.00
AR	303 K	4.9667	16.8752	MI	303 K	4.8048	15.9802
	363 K	4.9681	16.9011		363 K	4.8074	16.0037
	α ($10^{-6}\ K^{-1}$)	4.70	25.60		α ($10^{-6}\ K^{-1}$)	9.02	24.50
FH	303 K	4.9795	16.9344				
	363 K	4.9832	16.9548				
	α ($10^{-6}\ K^{-1}$)	12.40	20.10				

The 014, 006, 110 and 113 reflections of calcite and 014, 006, 015 and 110 reflections of dolomite recorded in the Bragg angle region between 27 and 42° 2θ were selected to calculate the lattice parameters at 303 and 363 K. In general, calcitic and dolomitic marbles (at 303 K) show close similarity between their lattice parameters (*a* and *c*) and the related measurements for single crystals of calcite and dolomite, although some length differences can be observed (Table 4).

Table 5 summarizes the lattice parameters (Å) obtained in the seven marbles at 303 and 363 K. The linear thermal expansion coefficient (α_a and α_c) measured according to the length changes produced along the *a* and *c* axes when the temperature increases (from 303 to 363 K) was calculated in the calcite and/or dolomite minerals present in each marble. The main change was in the value of the α_c parameter, which indicates that the maximum thermal expansion coefficient in all the marbles is along their *c* axis. WM showed the highest value ($25.7 \times 10^{-6}\ K^{-1}$), followed by TM, AR, FH, IB and MI, while YM showed the lowest thermal expansion value ($9.8 \times 10^{-6}\ K^{-1}$).

Not all marbles displayed similar thermal expansion coefficients. In WM the maximum thermal expansion of calcite fits quite well with its maximum thermal expansion along the *Z*-axis direction. This means that the thermal expansion of WM marble is directly controlled by the thermal expansion of its crystals and marble texture. The other marbles, TM, AR, MI, FH and IB, also showed high thermal expansion of their constituent minerals. However, texture differences could explain why there is no clear correlation with the thermal expansion of the marbles themselves, which is lower. YM showed the least correlation between its results; however, the behaviour of this marble may be influenced by the presence of calcite.

The thermal expansion coefficients of the seven studied marbles from Andalusia are slightly different from those of pure single crystals of calcite and dolomite (Krishna Rao *et al.*, 1967; Markgraf & Reeder, 1985; Reeder & Markgraf, 1986). However it is clear that the highest expansion values are

always obtained along the *c* axis in each sample, as has been found generally in calcitic marbles (Kleber, 1959). In contrast to the value obtained along the *a* axis for a calcite single crystal ($\alpha = -6 \times 10^{-6}\,K^{-1}$), all calcitic marbles also show expansion along this parameter (α_a). Nevertheless, this is not surprising considering that positive values were also recorded along two perpendicular directions of Yule marble after thermal tests carried out by Rosenholtz & Smith (1949). Measurement differences between lattice parameters obtained in a single crystal of calcite and dolomite and our measurements may be due to differences between their respective geological formation contexts. The measurement obtained for a single crystal shows ideal formation conditions, free from the effects of pressure, temperature and flow mobility, whereas marble minerals are the result of a range of different metamorphism processes. Therefore the presence of impurities and the development of dislocations in these minerals must also be taken into account.

Measurements obtained in powder samples provided the potential thermal expansion of calcite and dolomite crystals in a free state, *i.e.* without confining pressures. Thus, in addition to the idea that the rock fabric (grain sizes, grain boundaries, textures) is the main factor influencing thermal decay, the potential thermal expansion based on TXRD data indicates that another factor should be taken into account.

Of the seven Andalusian marbles studied in this work, it was confirmed that white Macael is the marble that shows the greatest dilatation and opening of micro-cracks as temperature increases. The thermal expansion coefficient, the fabric and the crystallographic preferred orientation are the main factors affecting the thermal behaviour of WM, which could lead to its granular decohesion after successive thermal cycles. Therefore, it is suggested that the exposure of this marble to the atmosphere must be defined and monitored.

5. Conclusions

The following conclusions regarding thermal behaviour of marbles can be drawn:

(i) The use of complementary analytical techniques to evaluate the thermal behaviour of different Andalusian marbles helped to obtain new data concerning parameters that influence marble thermal response when exposed to temperature changes.

(ii) Thermal expansion analyses revealed that the marble direction with the strongest damage due to temperature changes can be accurately predicted. However no relation was found to explain the residual strain observed in some heated marbles.

(iii) Ultrasound Vp and X-ray diffraction texture analyses demonstrated that anisotropies of physical parameters in all marbles are mainly controlled by the single-crystal anisotropy of their constituent minerals.

(iv) All Andalusian marbles underwent either changes or fractures in their grain boundaries under increasing temperature as revealed by ESEM inspection. This technique has demonstrated that formation and propagation of micro-cracks generated by thermal stress in marbles is crucial for determining how grain boundaries influence their thermal behaviour.

(v) Relevant thermal data were also obtained using thermo-X-ray diffraction, a novel application of this technique to characterize *in situ* temperature-aged marbles. Results obtained with this technique corroborate that the marble thermal expansion coefficient is directly related to the thermal expansion coefficients of its constituent minerals.

(vi) Confined calcite and dolomite crystals in marble samples have different thermal expansion coefficients depending on specific crystallographic orientation.

(vii) We also suggest that the existence of impurities and the presence of dislocations in single calcite or dolomite crystals in each marble can affect thermal behaviour.

This research was funded by the research projects FQM 1635 and MAT2008-06799-C03-03, the Integrated Action HA 2007-0012, RNM-04169, and Research Group RNM-179 (Junta de Andalucía, Spain). We thank Daniel Martín-Ramos for his assistance with thermo-X-ray diffraction analyses.

References

Althoff, P. L. (1977). *Am. Mineral.* **62**, 772–783.
Álvarez de Buergo, M. (2008). *Actas de las III Jornadas Técnicas. Durabilidad y Conservación de Materiales Tradicionales Naturales del Patrimonio Arquitectónico*, pp. 85–106. Cáceres: Instituto Tecnológico de Rocas Ornamentales y Materiales de Construcción.
ASTM (2005). *ASTM D2845-05. Standard Test Method for Laboratory Determination of Pulse Velocities and Ultrasonic Elastic Constants of Rock.* ASTM International, West Conshohocken, PA, USA.
Bello, M. A., Martín, L. & Martín, A. (1992). *Mater. Construcc.* **225**, 23–30.
Benavente, D., Cultrone, G. & Gómez-Heras, M. (2008). *Eur. J. Mineral.* **20**, 673–685.
Benavente, D., Martínez-Martínez, J., Cueto, N. & García del Cura, M. A. (2007). *Eng. Geol.* **94**, 215–226.
Bortz, S. A., Erlin, B. & Monk, C. B. (1988). *New Stone Technology, Design, and Construction for Exterior Wall Systems*, ASTM STP 996, edited by B. Donaldson, pp. 11–31. Philadelphia: American Society for Testing and Materials.
Bunge, H. J. (1985). *Preferred Orientation in Deformed Metals and Rocks: An Introduction to Modern Texture Analysis*, edited by H. R. Wenk, pp. 507–525. Orlando: Academic Press.
Burkhard, M. (1993). *J. Struct. Geol.* **15**, 351–368.
Cardell, C., Sánchez-Navas, A., Olmo-Reyes, F. J. & Martín-Ramos, J. D. (2007). *Anal. Chem.* **79**, 4455–4462.
Dahms, M. & Bunge, H. J. (1989). *J. Appl. Cryst.* **22**, 439–447.
Dandekar, D. P. (1968). *Phys. Rev.* **172**, 873–877.
Díaz-Aspiroz, M., Castro, A., Fernández, C., López, S., Fernández Caliani, J. C. & Moreno-Ventas, I. (2004). *J. Iber. Geol.* **30**, 23–51.
Espinosa, J., Villegas, R., Ager, F. & Gómez Tubío, B. (2002). *Actas del I Congreso del GEIIC. Conservación del Patrimonio: Evolución y Nuevas Perspectivas*, pp. 335–341. Valencia: Grupo Español IIC.
Fredrich, J. T. & Wong, T. F. (1986). *J. Geophys. Res.* **91**, 12743–12764.
Gómez-Heras, M., Smith, B. J. & Fort, R. (2006). *Geomorphology*, **78**, 236–249.
Guyader, J. & Denis, A. (1986). *Bull. Eng. Geol.* **33**, 49–55.

Hartley, G. & Mucci, A. (1996). *Geochim. Cosmochim. Acta*, **60**, 315–324.
Kessler, D. W. (1919). *Physical and Chemical Tests on the Commercial Marbles of the United States*, Technologic Papers of the Bureau of Standards No. 123. Washington, DC: US Government Printing Office.
Kleber, W. (1959). *Einführung in die Kristallographie.* Berlin: VEB Verlag Technik.
Koch, A. & Siegesmund, S. (2004). *Environ. Geol.* **46**, 350–363.
Krishna Rao, K. V., Nagender Naidu, S. V. & Satyanarayana Murthy, K. (1967). *J. Phys. Chem. Solids*, **29**, 245–248.
Lapuente, P., Preite-Martinez, M., Turi, B. & Blanc, P. (2002). *Asmosia 5: Interdisciplinary Studies on Ancient Stone*, edited by J. J. Hermann, N. Hertz & R. Newman, pp. 152–162. London: Archetype Publications.
Leiss, B. & Ullemeyer, K. (1999). *Z. Ges. Geowiss.* **152**, 259–274.
Leiss, B. & Ullemeyer, K. (2006). *11. Symposium, Tektonik, Struktur und Kristallingeologie*, edited by S. L. Philipp, B. Leiss, A. Vollbrecht, D. Tanner & A. Gudmundsson, pp. 128–130. Göttingen: Universitätsverlag.
Leiss, B. & Weiss, T. (2000). *J. Struct. Geol.* **22**, 1737–1745.
Logan, J. M., Hasted, M., Lehnert, D. & Denton, M. (1993). *Int. J. Rock Mech. Min. Sci. Geomech. Abstr.* **7**, 1531–1537.
Luque, A., Cultrone, G., Mosch, S., Siegesmund, S., Sebastián, E. & Leiss, B. (2010). *Eng. Geol.* **115**, 209–216.
Luque, A., Ruiz-Agudo, E., Cultrone, G., Sebastián, E. & Siegesmund, S. (2011). *Environ. Earth Sci.* **62**, 1375–1386.
Markgraf, S. A. & Reeder, R. J. (1985). *Am. Mineral.* **70**, 590–600.
Martínez-Martínez, J. (2008). PhD thesis, University of Alicante, Spain.
Martín-Ramos, J. D. (2004). *XPowder. Qualitative, Quantitative and Microtextural Powder X-ray Diffraction Analysis*, http://www.xpowder.com.
Matthies, S. & Vinel, G. W. (1982). *Phys. Status Solidi (b)*, **112**, K111–K114.
Monk, C. B. (1985). *Proceedings of the Third North American Masonry Conference*, pp. 191–227. The University of Texas at Arlington.
Padilla, A. (1999). *HABIS*, **30**, 271–281.
Passchier, C. W. & Trouw, R. A. J. (1996). *Microtetectonics*. Berlin, Heidelberg, New York: Springer.
Paterson, M. S. & Weiss, L. E. (1961). *Geol. Soc. Am. Bull.* **72**, 841–882.
Rayleigh, Lord (1934). *Proc. R. Soc. London*, **19**, 266–279.
Reeder, R. J. & Markgraf, S. A. (1986). *Am. Mineral.* **71**, 795–804.
Rodríguez-Gordillo, J. & Sáez-Pérez, M. P. (2010). *Mater. Construcc.* **60**, 127–141.
Rosenholtz, J. L. & Smith, D. T. (1949). *Am. Mineral.* **34**, 846–854.
Royer Carfagni, G. (1999). *Int. J. Rock Mech. Min. Sci.* **36**, 119–126.
Sáez Pérez, M. P. (2003). PhD thesis, University of Granada, Spain.
Sáez-Pérez, M. P. & Rodriguez-Gordillo, J. (2009). *Contruct. Build. Mater.* **23**, 2121–2126.
Sáncho-Gómez, C. (2006). *Papeles Partal*, **3**, 9–48.
Sanz de Galdeano, C. & López-Garrido, A. C. (2003). *Rev. Soc. Geol. Esp.* **16**, 135–149.
Siegesmund, S., Ruedrich, J. & Koch, A. (2008). *Environ. Geol.* **56**, 473–494
Siegesmund, S., Ullemeyer, K. & Weiss, T. (2000). *Int. J. Earth Sci.* **89**, 170–182.
Siegesmund, S., Weiss, T. & Schegg, T. (2000). *9th International Congress on Deterioration and Conservation of Stone, Venice, Italy*, pp. 205–213. Amsterdam: Elsevier.
Siegesmund, S., Weiss, T., Vollbrecht, A. & Ullemeyer, K. (1999). *Z. Dtsch. Geol. Ges.* **150**, 237–257.
Steinfink, H. & Sans, F. J. (1959). *Am. Mineral.* **44**, 679–682.
Sternbeck, J. (1997). *Geochim. Cosmochim. Acta*, **61**, 785–793.
Strohmeyer, D. (2003). PhD thesis, University of Göttingen, Germany.
Strohmeyer, D. & Siegesmund, S. (2002*a*). *Natural Stone, Weathering Phenomena, Conservation Strategies and Case Studies*, edited by S. Siegesmund, T. Weiss & A. Vollbrecht, pp. 115–135. London: Geological Society.
Strohmeyer, D. & Siegesmund, S. (2002*b*). *Geol. Soc. Spec. Publ.* **205**, 114–135.
Thomasen, S. E. & Ewart, C. S. (1984). *Third International Conference on Durability of Building Materials and Components*, pp. 313–323. Espoo: American Society for Testing and Materials.
Titiloye, J. O., De Leeuw, N. H. & Parker, S. C. (1998). *Geochim. Cosmochim. Acta*, **15**, 2637–2641.
Torres-Roldán, R. (1979). *Am. J. Sci.* **279**, 19–51.
Weiss, T., Siegesmund, S. & Fuller, E. R. (2002). *Natural Stone, Weathering Phenomena, Conservation Strategies and Case Studies*, S. Siegesmund, T. Weiss & A. Vollbrecht, pp. 89–102. London: Geological Society.
Weiss, T., Siegesmund, S. & Fuller, E. R. (2003). *Build. Environ.* **38**, 1251–1260.
Weiss, T., Siegesmund, S., Kirchner, D. & Sippel, J. (2004). *Environ. Geol.* **46**, 402–413.
Weiss, T., Siegesmund, S. & Rasolofosaon, P. N. J. (2000). *9th International Congress on Deterioration and Conservation of Stone, Venice, Italy*, pp. 215–224. Amsterdam: Elsevier.
Wenk, H. R., Venkitasubramanyan, C. S., Baker, D. W. & Turner, F. J. (1973). *Contrib. Mineral. Petrol.* **38**, 81–114.
Widhalm, C., Tschegg, E. & Eppensteiner, W. (1996). *J. Perform. Constr. Facil. ASCE*, **11**, 35–40.
Winkler, E. M. (1996). *Int. J. Rock Mech. Min. Sci. Geomech. Abstr.* **33**, 215–218.
Wogelius, R. A., Fraser, D. G., Wall, G. R. T. & Grime, G. W. (1997). *Geochim. Cosmochim. Acta*, **61**, 2037–2051.
Zeisig, A., Siegesmund, S. & Weiss, T. (2002). *Natural Stone, Weathering Phenomena, Conservation Strategies and Case Studies*, S. Siegesmund, T. Weiss & A. Vollbrecht, pp. 65–80. London: Geological Society.
Zezza, U., Massara, E. P., Massa, V. & Venchiarutti, D. (1985). *Proceedings of the 5th International Congress on Deterioration and Conservation of Stone*, pp. 131–140. Lausanne: Presses Polytechniques et Universitaires Romandes.
Zezza, U. & Sebastián-Pardo, E. (1992). *I Congreso Internacional Rehabilitación del Patrimonio Arquitectónico y Edificación*, Tomo I, pp. 153–60. San Cristobal de la Laguna: Nueva Grafica.